Available online at www.sciencedirect.com
ScienceDirect
Journal of Solid State Chemistry 179 (2006) 2809–2818
JOURNAL OF SOLID STATE CHEMISTRY
www.elsevier.com/locate/jssc

# Development and application of high strength ternary boride base cermets

Ken-ichi Takagi*

*Technical Research Laboratory, Toyo Kohan Co., Ltd., 1296 Higashitoyoi, Kudamatsu 744-8611, Japan*

Received 20 September 2005; received in revised form 5 December 2005; accepted 10 January 2006
Available online 10 February 2006

**Abstract**

Reaction boronizing sintering is a novel strategy to form a ternary boride coexisting with a metal matrix in a cermet during liquid phase sintering. This new sintering technique has successfully developed world first ternary boride base cermets with excellent mechanical properties such as $Mo_2FeB_2$, $Mo_2NiB_2$ and WCoB base ones.

In these cermets $Mo_2FeB_2$ and $Mo_2NiB_2$ base ones consist of a tetragonal $M_3B_2$ ($M$: metal)-type complex boride as a hard phase and a transition metal base matrix. The cermets have already been applied to wear resistant applications such as injection molding machine parts, can making tools, and hot copper extruding dies, etc.

This paper focuses on the characteristics, effects of the additional elements on the mechanical properties and structure, and practical applications of the ternary boride base cermets.


*Keywords:* Boride base cermet; Ternary boride; Mechanical properties; Microstructure; Wear resistance; Corrosion resistance; Application

## 1. Introduction

For industrial application, wear resistant materials should have a wide range of properties such as high strength, high toughness, corrosion and oxidation resistance, electrical and thermal conductivity, etc. Among very hard materials, borides, especially transition metal borides possess high hardness, high melting points and electrical conductivity. Hence, borides are promising candidates for wear resistant applications. But borides show poor sinterability, extreme brittleness and strong reactivity with metals, which are notorious disadvantages to form solid structures.

As shown in the Mo–Fe–B ternary phase diagram [1] (Fig. 1), we recognize that among many binary and ternary borides, the $Mo_2FeB_2$ ternary boride has the possibility of coexisting with a metal matrix of Fe or Mo. In addition to $Mo_2FeB_2$, some ternary borides, for example $Mo_2NiB_2$, $W_2NiB_2$, WCoB, MoCoB, etc., are candidates for the hard phase of the boride base cermets. The ternary phase diagram suggests that enhancement of the reaction between a binary boride and metallic elements during sintering leads to a novel liquid-phase sintering technique of boride base cermets associated with in situ reacting formation of ternary borides in a metal matrix. Fig. 2 shows the new sintering sequence named reaction-boronizing sintering [2,3]. The sequence starts with a powder mixture of a binary boride and pure metals or alloys. At the second stage, by raising the temperature a ternary boride is formed at the contacting points of these powders by solid-state reactions prior to liquid formation. This stage is the key of the sintering sequence. At the third stage, a quasi-eutectic reaction between the ternary boride and the metal matrix results in the formation of eutectic liquid and considerable densification occurs by particle rearrangement and solution/reprecipitation of the ternary boride to reach full density. Finally, a sintered compact has the ideal two-phase structure of the ternary boride and the metal matrix.

This reaction boronizing sintering has successfully developed three ternary boride base cermets: $Mo_2FeB_2$-Fe [4], $Mo_2NiB_2$-Ni [5] and WCoB-Co [6]. These cermets

*Corresponding author. Fax: +81 833 43 0295.
*E-mail address:* u4381@toyokohan.co.jp.

0022-4596/$ - see front matter © 2006 Elsevier Inc. All rights reserved.
doi:10.1016/j.jssc.2006.01.023

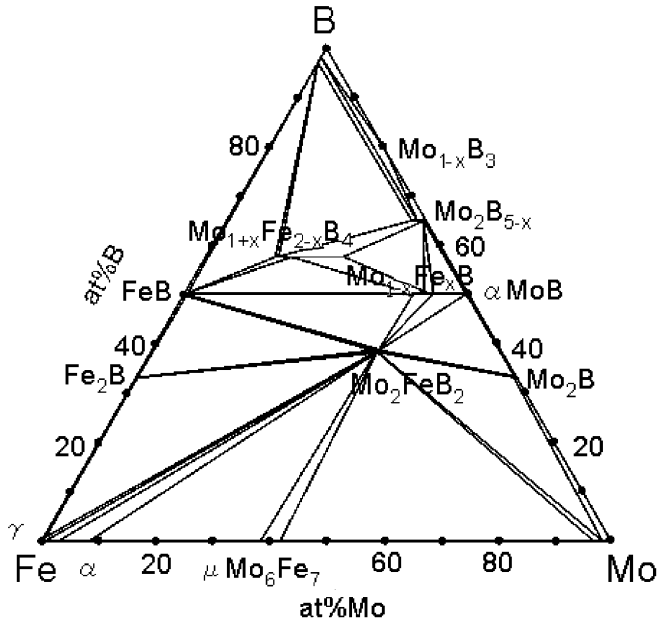


Fig. 1. Isothermal cross section of Mo–Fe–B at 1323 K.

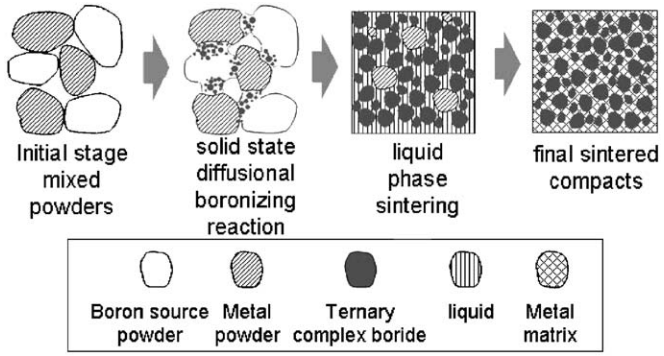


Fig. 2. Schematic illustration of reaction boronizing sintering involving liquid phase to form a ternary boride base cermet.

show excellent mechanical properties, wear and corrosion resistance and have been applied to injection machine parts, can making tools, hot copper extruding dies, etc. This paper focuses on the characteristics, effects of the additional elements on the mechanical properties and structure and practical applications of $Mo_2FeB_2$ and $Mo_2NiB_2$ ternary boride base cermets.

## 2. $Mo_2FeB_2$ ternary boride base cermet

$Mo_2FeB_2$ ternary boride base cermets have good mechanical properties, excellent corrosion and wear resistance and have been successfully applied to various kinds of wear resistant parts such as injection molding machine parts. In this section, we investigated the microstructure, physical properties, wear resistance and bonding characteristics of the representative cermets.

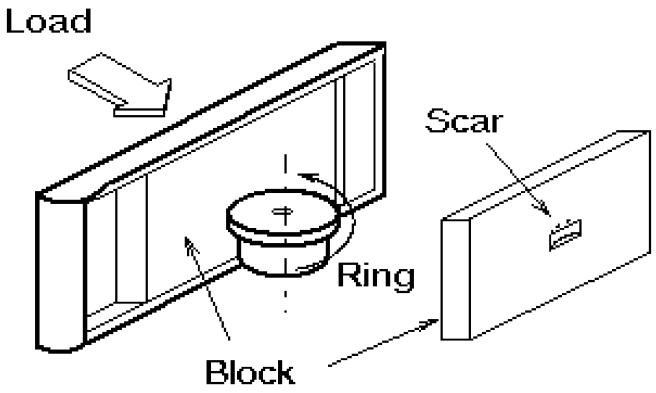


Fig. 3. Schematic illustration of Ogoshi sliding wear test.

### 2.1. Experimental procedure

Typical $Mo_2FeB_2$ ternary boride base cermets V30 with the composition of Fe–6.0B–47.5Mo–2.9Ni–2.4Cr (mass%) and V50 with the composition of Fe–4.3B–35.1 Mo–2.9Ni–8.1Cr–3.8W (mass%) were mainly used for the investigation. The powder mixtures prepared from Fe–17.7B–0.2C (mass%) alloy powder, pure Mo, carbonyl Ni, carbonyl Fe and Pure Cr were ball-milled in acetone to an average particle size of about 1 μm. After drying the milled powders were pressed to green compacts and sintered in vacuum for 1.2 ks at 1498–1523 K. The microstructure of the sintered cermets was investigated by means of scanning electron microscope (SEM) and Auger electron spectroscopy (AES). Physical properties such as transverse rupture strength (TRS), Rockwell "A" hardness, fracture toughness, Young's modulus and thermal expansion coefficient of the typical $Mo_2FeB_2$ boride base cermets were measured.

For the study of metal to metal compatibility, we employed the Ogoshi sliding wear test as shown in Fig. 3. In this test a block specimen surface was forced against a rotating ring specimen under the condition of sliding distance of 600 m and with a final load of 185 N. After the test wear volume loss both of the block and ring specimens was measured and used to calculate the specific wear rate per unit load and unit sliding distance. Furthermore, worn surface of the block specimens and wear debris were investigated by means of SEM and X-ray diffraction (XRD). Bonding interfaces with steel were also studied.

### 2.2. Microstructure

Fig. 4 shows a typical SEM micrograph and Auger spectra at two analysis points of the cermet. The spectra indicate that light gray particles contain Mo, Fe, B and Cr. These particles are $Mo_2FeB_2$-type complex boride; that is $(Mo, Fe, Cr)_3B_2$. The dark phase containing Fe, Cr, Ni and small amounts of Mo is the ferrous matrix with a stainless steel like composition. The ternary boride particles are uniformly distributed in the ferrous matrix. The ferrous

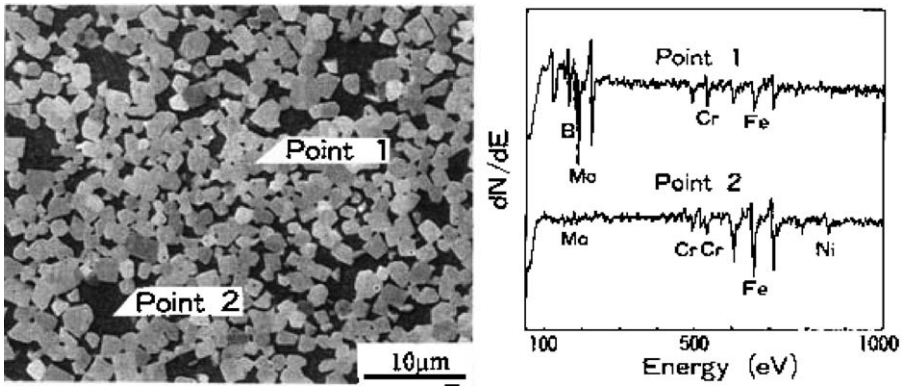


Fig. 4. SEM micrograph and Auger spectra of $Mo_2FeB_2$ boride base cermet V30.

Table 1
Physical properties of the $Mo_2FeB_2$ base cermets V30 and V50

| Grade | V 30 | V 50 |
|---|---|---|
| Density (kg/m$^3$) | 8.2 | 8.3 |
| Hardness ($R_A$) | 89 | 85 |
| TRS (GPa) | 2.05 | 2.25 |
| Young's modulus (GPa) | 350 | 300 |
| Fracture toughness (MN/m$^{3/2}$)[a] | 19.2 | 30.0 |
| Thermal expansion coefficient ($\times 10^{-6}$/K) | 8.5 | 10.5 |

[a]Indentation method.

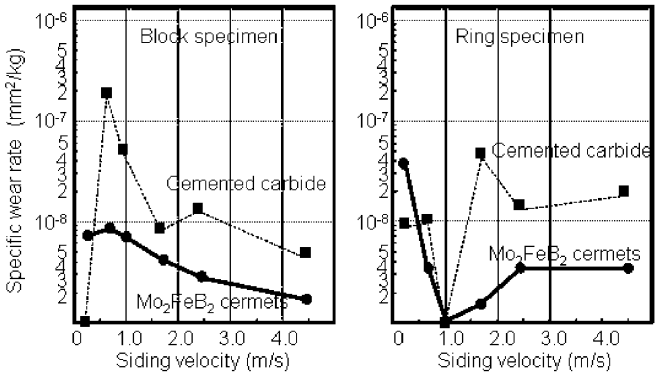


Fig. 5. Specific wear rate of $Mo_2FeB_2$ base cermet V30 and cemented carbide WC-10Co block and ring specimens against themselves.

matrix of the $Mo_2FeB_2$ boride base cermet becomes ferrite, martensite or austenite depending on its Cr and Ni content.

### 2.3. Physical properties

Table 1 lists physical properties of the $Mo_2FeB_2$ boride base cermets V30 and V50. Hardness and TRS are similar to those of cemented carbides. On the other hand density is approximately three-fifth of cemented carbides and similar to those of steels. The cermets have relatively high fracture toughness compared to cemented carbides and a thermal expansion coefficient close to those of steels.

### 2.4. Wear resistance

Fig. 5 shows specific wear rates of the block and ring specimens of the $Mo_2FeB_2$ boride base cermet (V 30) and the cemented carbide (WC-10Co) against themselves as a function of sliding velocity. The boride base cermet V 30 exhibits equivalent or better sliding wear resistance against itself than the cemented carbide at almost all sliding velocities. Furthermore, the cermet does less damage to the mating material than the cemented carbide.

Fig. 6 indicates the X-ray diffraction results of wear debris obtained from the cermet at various sliding velocities. Only $Mo_2FeB_2$ is detected at low sliding velocity. Higher sliding velocities yield several oxides such as $MoO_2$, small amounts of $B_2O_3$ and $Fe_3O_4$. In the case of the cemented carbide no oxide and only WC were detected at all sliding velocities.

SEM micrographs of wear debris and worn surfaces of the block specimens of the cermet and the cemented carbide at 1.65 m/s are shown in Fig. 7. The cermet yields small roll shape wear debris. This is thought to be formed during sliding due to the low melting point of oxides such as $MoO_2$, $B_2O_3$ and $Fe_3O_4$. These wear debris increases with increasing sliding velocity. On the other hand, the cemented carbide forms larger plate like wear debris than the cermet. Moreover, crushed WC particles are found on the worn surface. The crushed particles may cause self-abrasive wear during sliding and enhance the specific wear rate of the cemented carbide. Consequently, oxides formed on the cermets may prevent the adhesion between the same block and ring specimens and may act as a lubricant during sliding. This wear behavior contributes to the excellent performances of the injection molding machine parts made by the cermets.

### 2.5. Bonding properties

Most of the injection machine parts composed of the cermet have a bimetallic structure because of strengthening, toughening and lowering cost. The cermet can be bonded to steel with solders and also diffusion-bonded by

heating the sintered body with a coupling material without solder. Furthermore, the sinter-bonding technique where the sintering of the green compact and bonding between the sintering compact and the coupling material take place simultaneously is applicable. This technique realizes a relatively thin wear resistant hard layer by using a green sheet or slurry coating of the cermet.

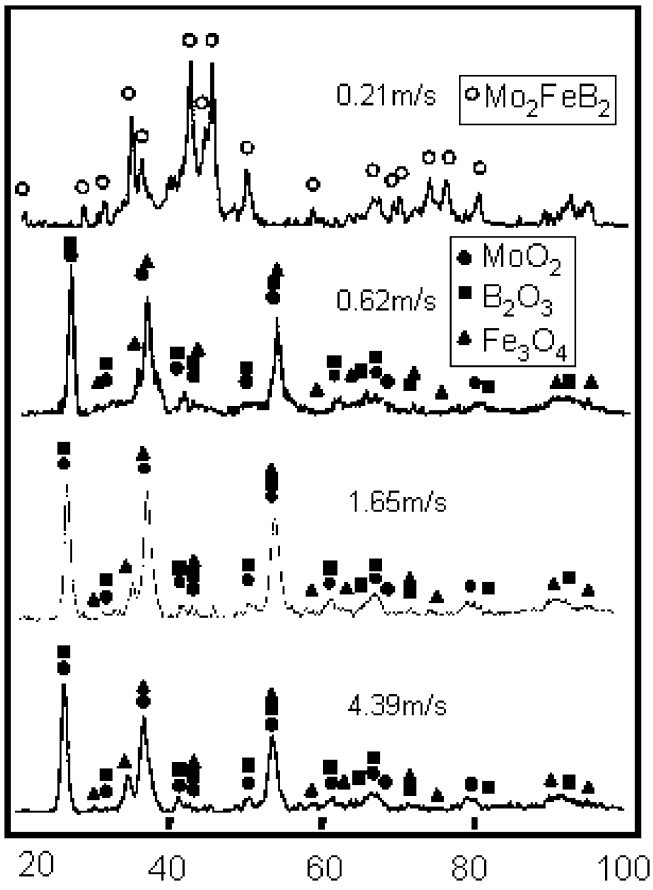


Fig. 6. Cu-$K\alpha$ X-ray diffraction patterns of the wear debris obtained from the block specimen of $Mo_2FeB_2$ cermet V30 slid against the same cermet ring at various sliding velocities.

Fig. 8 shows the SEM micrograph of the sinter-bonded interface between the cermet V 50 and a chromium molybdenum steel JIS SCM 440 (AISI 4140 equivalent). This combination is used for the bimetallic screw of a plastic injection-molding machine. The micrograph indicates that perfect metallurgical bonding is realized at the interface. The formation of a Fe–B or Fe–$Mo_2FeB_2$ eutectic liquid phase at the interface makes possible the diffusion and sinter-bonding processing. The relatively high thermal expansion coefficient of the cermet contributes to the realization of these bonding techniques by reducing residual thermal stress.

## 3. $Mo_2NiB_2$ ternary boride base cermet

By adopting $Mo_2NiB_2$ ternary boride as a hard phase in Fig. 9 [7], we developed $Mo_2NiB_2$ ternary boride base cermets with a Ni base matrix. The cermets have excellent corrosion resistance in addition to good mechanical properties and wear resistance. In this section, we studied the effect of Cr, V and Mn addition on the mechanical properties and phase formation of the cermets.

### 3.1. Effect of Cr and V addition

#### 3.1.1. Experimental procedure

Table 2 shows the composition of the three model cermets used in this investigation. The powder mixtures prepared from pure Mo, carbonyl Ni, MoB, CrB and $VB_2$ were ball-milled in acetone to an average particle size of about 1 μm. After drying the milled powders were pressed

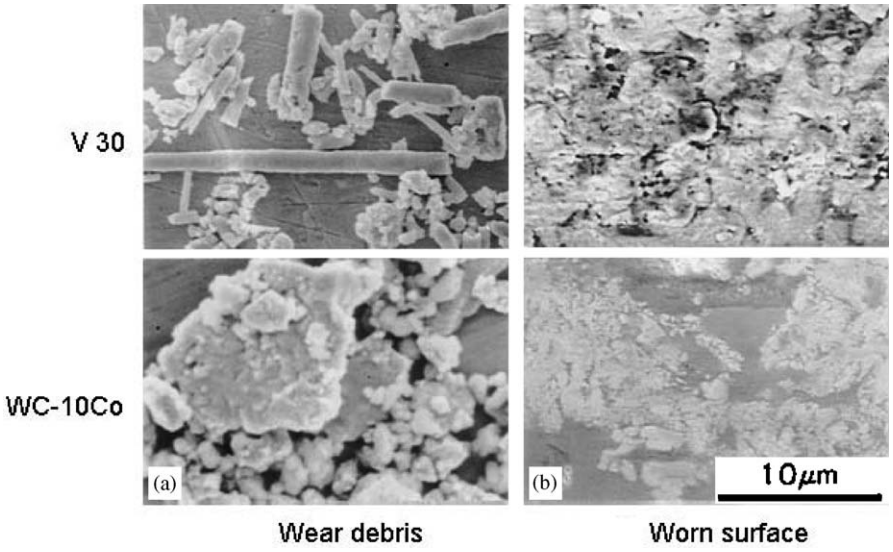


Fig. 7. SEM micrographs of (a) wear debris and (b) worn surfaces of the block specimens of $Mo_2FeB_2$ cermet V30 and WC-10Co at a sliding velocity of 1.65 m/s.

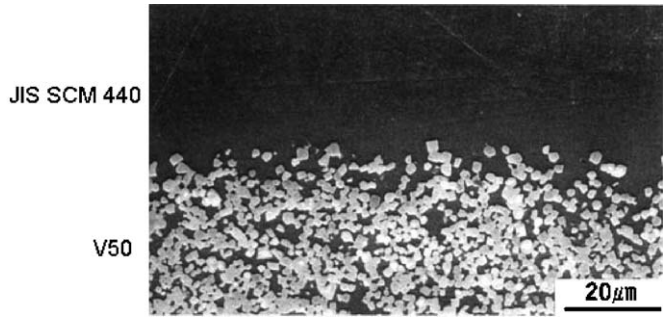


Fig. 8. SEM micrograph of sinter-bonding interface between $Mo_2FeB_2$ cermet V50 and JIS SCM 440.

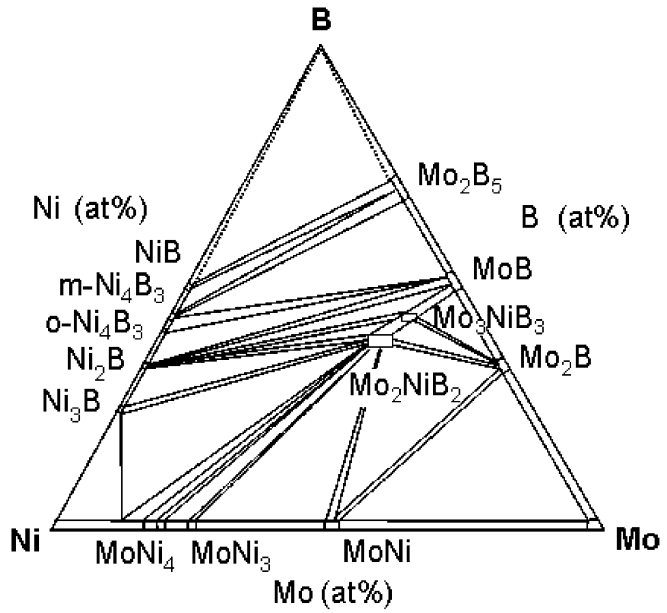


Fig. 9. Isothermal cross section of Mo–Ni–B at 1073 K.

Table 2
Compositions of the investigated $Mo_2NiB_2$ boride base model cermets

| | Mass% | | | | |
|---|---|---|---|---|---|
| | *B* | Mo | Cr | V | NI |
| Basic cermet | 6.0 | 58.6 | — | — | Bal. |
| Cr added cermet | 6.0 | 58.6 | 10.0 | — | Bal. |
| V added cermet | 6.0 | 58.6 | — | 0.0 | Bal. |

to green compacts and sintered in vacuum for 1.2 ks at 1573 K. The microstructure of the sintered cermets was investigated by means of SEM, AES and XRD. TRS, Rockwell "A" hardness and fracture toughness of the cermets were measured.

### 3.1.2. Mechanical properties

TRS and hardness of the three model cermets are shown in Fig. 10. Cr and V additions improve the TRS drastically

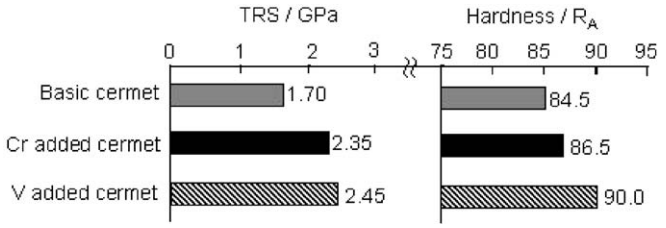


Fig. 10. Transverse rupture strength (TRS) and hardness of three $Mo_2NiB_2$ boride base model cermets.

from 1.70 GPa for basic cermet to 2.35 and 2.45 GPa for Cr and V added cermets, respectively. Both elements especially V also increase the hardness markedly from 84.5$R_A$ to 86.5 and 90.0$R_A$. These TRS and hardness values are comparable to those of cemented carbides.

### 3.1.3. Microstructure

Fig. 11 shows the typical microstructures of the three model cermets using SEM back scattered electron images. The coarse rectangular $Mo_2NiB_2$ complex boride (light gray phase) and the Ni base matrix (dark phase) are observed in the micrograph of the basic cermet. These SEM images also indicate that the particle size of the complex boride becomes small with the addition of Cr and V. Moreover, the addition of Cr and V changes the shape of the boride from rectangular to spherical. The distribution of alloying elements in the cermets was studied by AES. In the case of Cr and V added cermets the $Mo_2NiB_2$ boride (Points 1 and 3) contains Mo, B, Ni and Cr or V. The boride in these cermets is considered to be (Mo, Ni, Cr or V)$_3B_2$ complex boride (hereafter $M_3B_2$ (*M*: metal)-type boride). The matrix (Points 2 and 4) contains Mo, Ni and Cr or V. Cr and V are present in both of the complex boride and the Ni base matrix. From the Auger spectra the content of both elements in the matrix is somewhat larger than that in the complex boride.

Fig. 12 shows the X-ray diffraction results of the three model cermets sintered at 1573 K for 1.2 ks in vacuum. The basic cermet consists of the orthorhombic $Mo_2NiB_2$ boride and Ni base matrix. On the other hand Cr and V addition causes a structural change of the $Mo_2NiB_2$ complex boride from orthorhombic to tetragonal. Furthermore, a small shift of the Ni reflection to a lower Bragg angle is detected. We note that Cr and V added cermets consist of an ideal two-phase structure with fine-grained spherical crystals of the tetragonal $Mo_2NiB_2$ complex boride and the Ni base matrix.

### 3.1.4. Structural analysis

Rietveld analysis was performed in order to investigate the crystal structure of the ternary boride phase, namely the orthorhombic $Mo_2NiB_2$ in basic cermet and the tetragonal $Mo_2NiB_2$ at 10 mass% Cr cermet. As shown in Table 3 the orthorhombic $Mo_2NiB_2$ was classified as space group No. 71. This result agrees well with the structure of

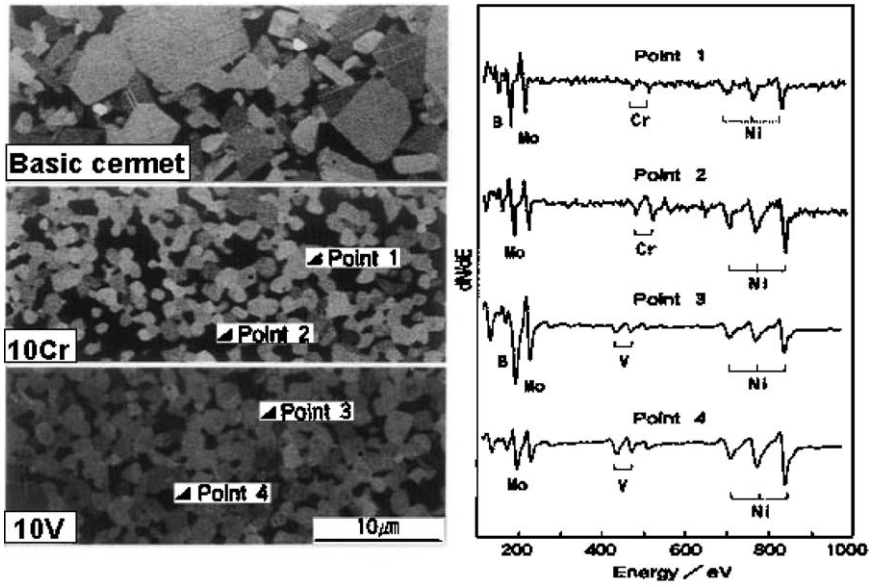


Fig. 11. Back-scattered electron images and Auger spectra of Ni–6B–58.6Mo–(0Cr, 10Cr and10 V) mass% cermets.

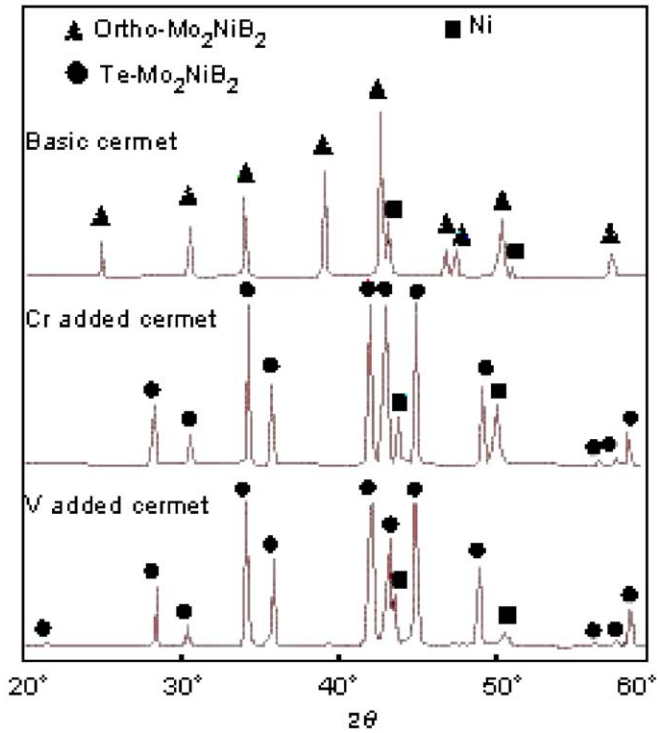


Fig. 12. Cu-$K\alpha$ X-ray diffraction patterns of Ni–6B–58.6Mo–(0Cr, 10Cr and 10 V) mass% cermets sintered at 1573 K for 1.2 ks in vacuum.

orthorhombic $W_2CoB_2$ reported by Rieger et al. [8]. The tetragonal $Mo_2NiB_2$-type boride was classified as space group No. 127, the same as $Mo_2FeB_2$ [9].

Schematic illustration of the orthorhombic $Mo_2NiB_2$ and the tetragonal $Mo_2NiB_2$ unit cells is shown in Fig. 13. Cr can substitute for Ni in the tetragonal structure. By comparison of these structures it is clearly seen that the orthorhombic $M_3B_2$ structure is more anisotropic than the tetragonal one.

Fig. 14 shows the grain shape ratio as a function of the interface energy ratio given by the {100} energy $\gamma_{100}$ divided by the mean energy $\gamma_{SL}$ calculated by Warren [10]. The equilibrium grain shape for a given energy ratio is given by those $r/a$ values which give a minimum value to the interface energy per unit volume assuming no planes besides {100} have energies significantly lower than the mean. These results suggest that the grain shape changes from near-spherical to perfect cubic takes place by small decrease in the degree of crystallographic isotropy through anisotropic surface energy. The change from spherical to rectangular grain shape in $M_3B_2$-type borides also corresponds with a decrease in isotropy of the crystal structure, which is in good agreement with Warren's results.

### 3.1.5. Summary of the effect of Cr and V addition

Cr and V addition caused the structural change of the $Mo_2NiB_2$ ternary boride from orthorhombic to tetragonal and resulted in a remarkable improvement of mechanical properties and structural refinement of the cermet. The high TRS of the Cr and V containing cermets is further attributed to the homogeneous distribution of the tetragonal $M_3B_2$ boride phase and the absence of the third phase. From these results it is believed that the formation of the tetragonal $M_3B_2$ is indispensable to obtain excellent mechanical properties.

## 3.2. Effect of Mn addition

The effect of Mn addition to the $Mo_2NiB_2$ ternary boride cermet was also investigated by using simple

Table 3
Structure determination of boride phases identified in Ni–6B–58.6Mo–(0 and 10)Cr mass% cermets

| Crystal system | ◆ Orthorhombic $M_3B_2$ | ◆ Tetragonal $M_3B_2$ |
|---|---|---|
| Symbol and no. of space group position | $D_{21}^{25}$-*Immm* (No. 71)<br>4Mo in 4*f*:<br>$x$,1/2,0; $\bar{x}$,1/2,0<br>with $x = 0.1994$<br>2Ni in 2*a*:<br>0.0.0<br>4B in 4*h*:<br>0,$y$,1/2; 0,$\bar{y}$,1/2<br>with $y = 0.2944$ | $D_{41}^{5}$-*P* 4/*mbm* (No. 127)<br>4Mo in 4*h*:<br>$x$, $x+1/2$,1/2; $\bar{x}$,$\bar{x}+1/2$,1/2<br>$\bar{x}+1/2$,$x$,1/2; $x+1/2$,$\bar{x}$,1/2<br>with $x = 0.1776$<br>2(Ni,Cr) in 2*a*:<br>0,0,0; 1/2,1/2, 0<br>4B in 4*g*:<br>$y$,$y+1/2$,0; $\bar{y}$,$\bar{y}+1/2$,0<br>$\bar{y}+1/2$,$y$,0;$y+1/2$,$\bar{y}$,0<br>with $y = 0.3794$ |

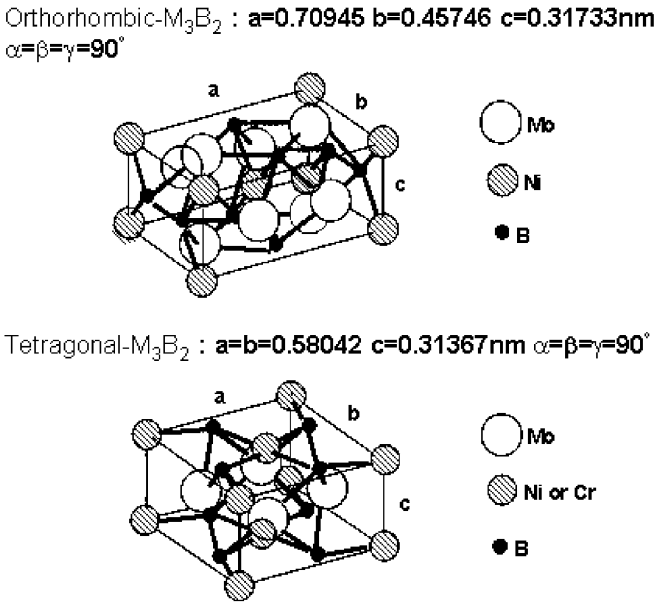


Fig. 13. Orthorhombic- and tetragonal-$M_3B_2$ unit cells observed in Ni–6B–58.6Mo–(0 and 10)Cr mass% cermets.

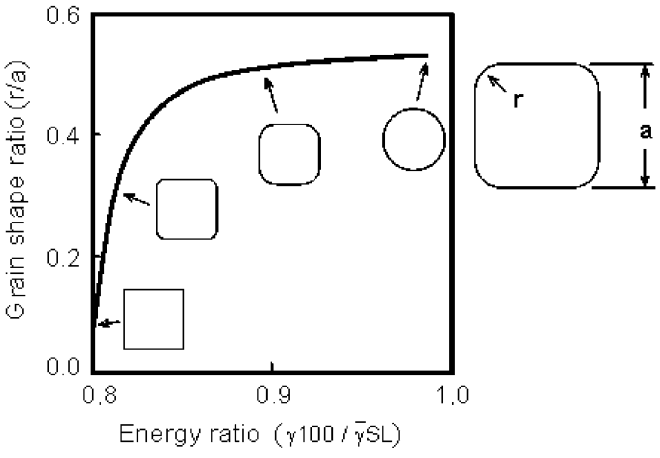


Fig. 14. The surface energy anisotropic effect on grain shape given by the ratio of the surface energy in the (100) direction divided by the mean surface energy.

$Mo_2NiB_2$ boride base model cermets with the composition of Ni–5B–53.3Mo–(0–10) Mn (mass%) and high strength V added cermets with the composition of Ni–4.5B–46.9 Mo–12.5V–(0–10) Mn (mass%). The experimental procedure was similar to that of Cr and V addition.

### 3.2.1. Structure property relationship in the Mn added $Mo_2NiB_2$ boride based cermets

Fig. 15 summarizes the effect of Mn addition on the mechanical properties and microstructure of the simple $Mo_2NiB_2$ boride cermets. Mn addition to the cermets also brings about mechanical property improvements and structural refinement at 5 mass% Mn. Fracture toughness is markedly improved at 10 mass% Mn due to the decrease of contiguity. Unlike Cr and V, addition Mn did not cause any structural change in the ternary boride and hence the boride phase in the cermet maintained its original orthorhombic structure.

The effects of Mn on the mechanical properties and microstructure of high strength V added $Mo_2NiB_2$ boride-based cermets are shown in Fig. 16. TRS reaches a maximum of 3.5 GPa at 2.5 mass% Mn and then decreases with increasing Mn content, while the hardness increases linearly up to $88R_A$ at 10 mass% Mn. The mean particle size of the boride decreases with increasing Mn content and shows a minimum at 7.5 mass% Mn in spite of the formation of some coarse particles observed in the back scattered electron images. Then, the particle size increases again at 10 mass% Mn because of extensive coarsening. The contiguity of the boride particles slightly increases up to 5 mass% Mn, and further increases with increasing Mn content. Independently the Mn content boride phase of the cermet used in this investigation maintained its tetragonal structure as a result of V addition.

### 3.2.2. Summary of the effect of Mn addition

High TRS values of the cermets obtained by Mn addition are attributed to the refinement and uniform distribution of the boride particles in the Ni base matrix. Mn addition is considered to improve wettability of the formed liquid phase and decreases the dihedral angle

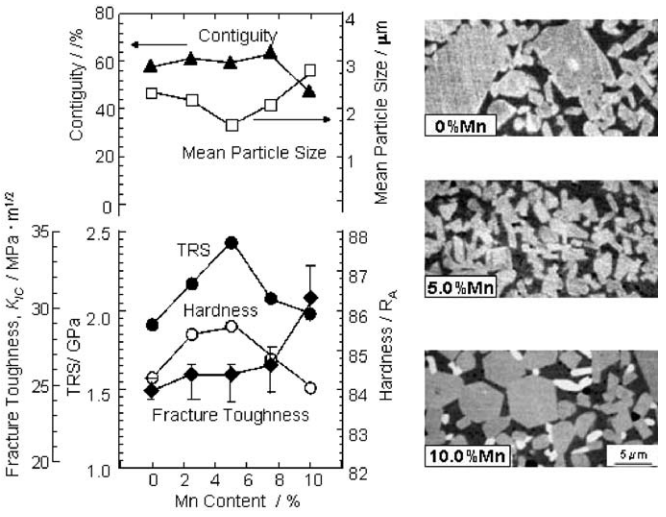


Fig. 15. Structure property relationship in Ni–5B–53.3Mo–*x*Mn mass% cermets.

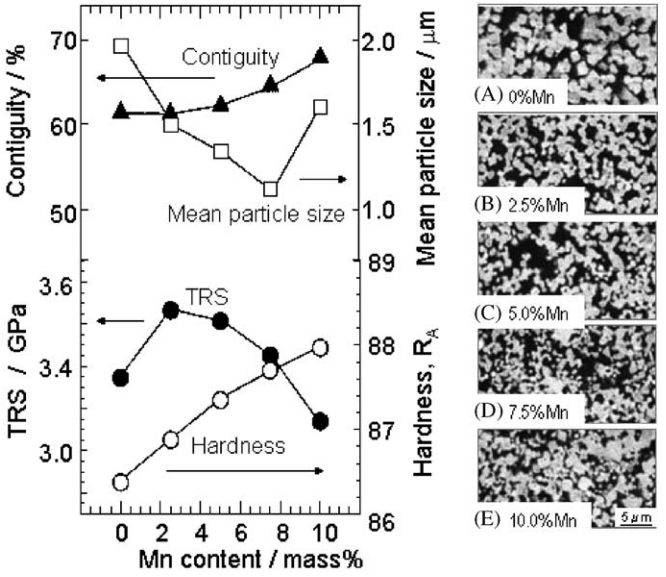


Fig. 16. Structure property relationship in Ni–4.5B–46.9Mo–12.5V–*x*Mn mass% cermets.

between boride and matrix phases and results in microstructural refinements during sintering. Moreover, Mn would show Rhenium ductilizing or solution softening, which is observed in a elements such as Cr, Mo and W with Re addition as mentioned by Klopp [11]. A very fine, ideal two-phase microstructure with homogeneous distribution of the tetragonal $Mo_2NiB_2$ phase in the matrix leads to high TRS values.

### 3.3. Development of highly corrosion resistant $Mo_2NiB_2$ boride cermets

Wear and corrosion become an everyday concern in injection molding processes. Engineering plastics and super

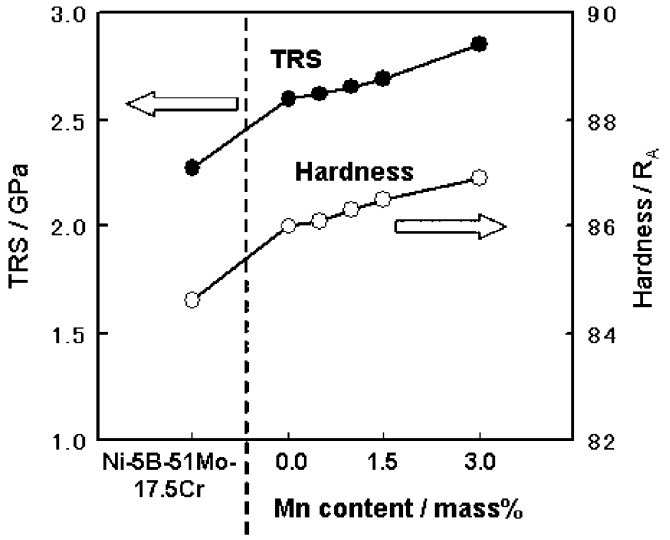


Fig. 17. TRS and hardness of Ni–5B–51Mo–17.5Cr and Ni–5B–51Mo–12.5Cr–5V–*x*Mn mass% cermets as functions of Mn content.

engineering plastics containing various kinds of fillers are widely used in injection molding. Among them fluorocarbon polymer is very corrosive due to the emission of hydrogen fluoride (HF) gas. This section focuses on the characteristics and corrosion test results of molten fluorocarbon resin on recently developed $Mo_2NiB_2$ boride-based cermets with multiple addition of Cr, V and Mn.

#### 3.3.1. Experimental procedure

In this investigation we used Ni–5B–51Mo–17.5Cr (mass%) and Ni–5B–51Mo–12.5Cr–5V–(0–3)Mn (mass%) cermets. The experimental procedure to study mechanical properties and microstructure was similar to that of Cr and V addition. We also studied the microstructure by means of transmission electron microscopy (TEM) and corrosion resistance in molten fluorocarbon resin at 673 K for 259.2 ks (72 h) (Fluorocarbon resin: Neoflon PFA, Daikin Industries Ltd.).

#### 3.3.2. Mechanical properties

Fig. 17 shows the TRS and hardness of the tested $Mo_2NiB_2$ boride-based cermets. Both TRS and hardness are improved by the replacement of 5 mass% Cr with V and increase with increasing Mn content.

#### 3.3.3. Microstructure

Back scattered electron images of the tested cermets are shown in Fig. 18. Multiple addition of V and Mn further decreases the boride particle grain size. A small amount of white phase is observed in V and Mn added cermets. X-ray diffraction results of the cermets are shown in Fig. 19. Regardless of Mn content all the cermets consist of tetragonal $M_3B_2$ complex boride and the Ni base matrix

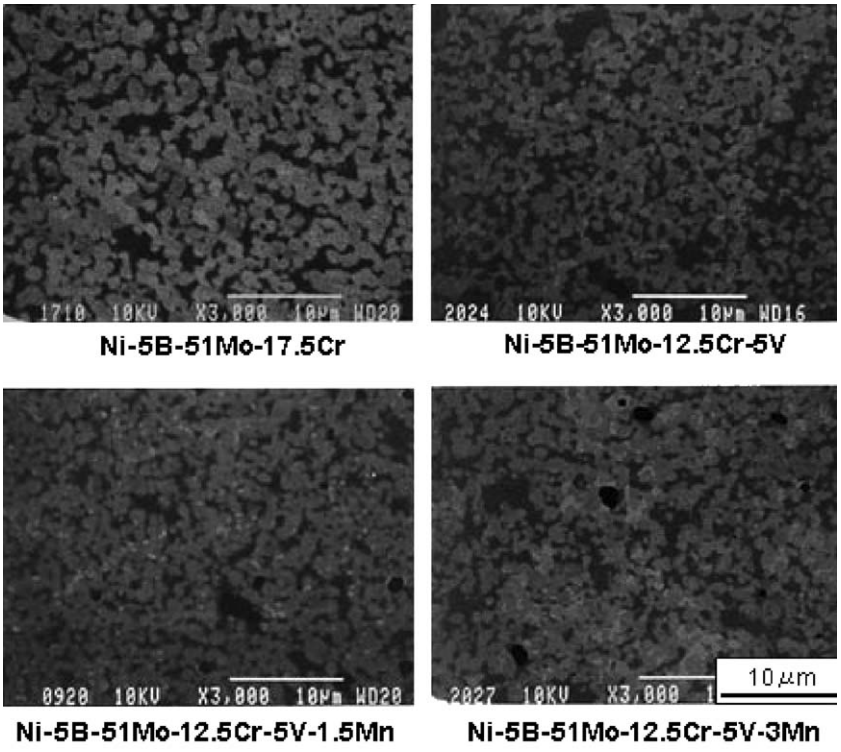


Fig. 18. Back scattered electron images of Ni–5B–51Mo–17.5Cr and Ni–5B–51Mo–12.5Cr–5V–*x*Mn mass% cermets.

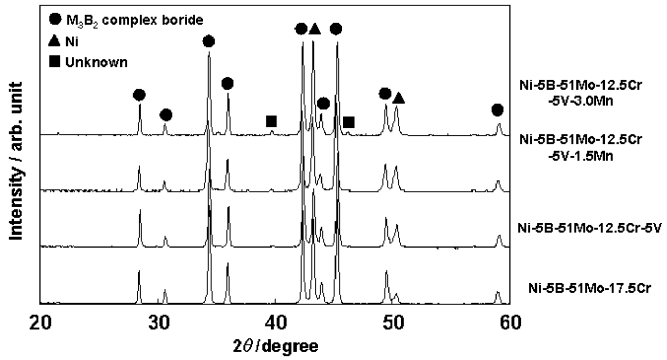


Fig. 19. Cu-Ka X-ray diffraction patterns of Ni–5B–51Mo–17.5Cr and Ni–5B–51Mo–12.5Cr–5V–*x*Mn mass% cermets.

due to Cr and V addition. A small amount of an unknown phase is observed in 3 mass% Mn containing cermet.

Fig. 20 shows thin foil electron micrographs and EDS spectra analyzed at three points of the 3 mass% Mn containing cermet. In addition to Mo and Ni, both boride (Point 2) and Ni base matrix (Point 1) contain some amount of Cr and V. The Mn partitioning is not clear in this study because the Mn spectrum overlaps with that of Cr. Point 3 contains a relatively large amount of Mo and Ni in addition to B, Cr, V and Mn. This phase corresponds to the white phase in the back-scattered electron image and is thought to be a $M_5B_3$ ($M$: metal)-type boride from the electron diffraction pattern.

### 3.3.4. Corrosion test result

As shown in Fig. 21 corrosion test results of the cermets together with comparative materials in the molten fluorocarbon resin reveal that the $Mo_2NiB_2$ boride-based cermet with multiple additions of Cr, V and Mn has far better corrosion resistance than the $Mo_2FeB_2$ base cermets and steels and is comparable to the superalloy Hastelly C. This result indicates that $Mo_2NiB_2$ boride-based cermets with mulitple additions of Cr, V and Mn have excellent performance in practical applications in injection molding.

## 4. Application

Ternary boride-based cermets have already been applied to many kinds of corrosion and wear resistant machine parts taking advantage of their excellent characteristics. Such applications are injection molding machine parts such as screws, barrels, reverse flow stop valves, etc., non-lubricant cylinder liners for compressed natural gas (CNG) and hydrogen pumps, can making tools, hot copper extruding dies, bearings for sea water pumps, cutters for heat sealers, drills for sand molds, etc. Many parts such as screws and drills are produced by using sinter-bonding and slurry coating techniques as well as by reaction boronizing sintering.

## 5. Summary

Borides have excellent intrinsic properties, such as high melting points, high hardness, magnetism, superconductivity,

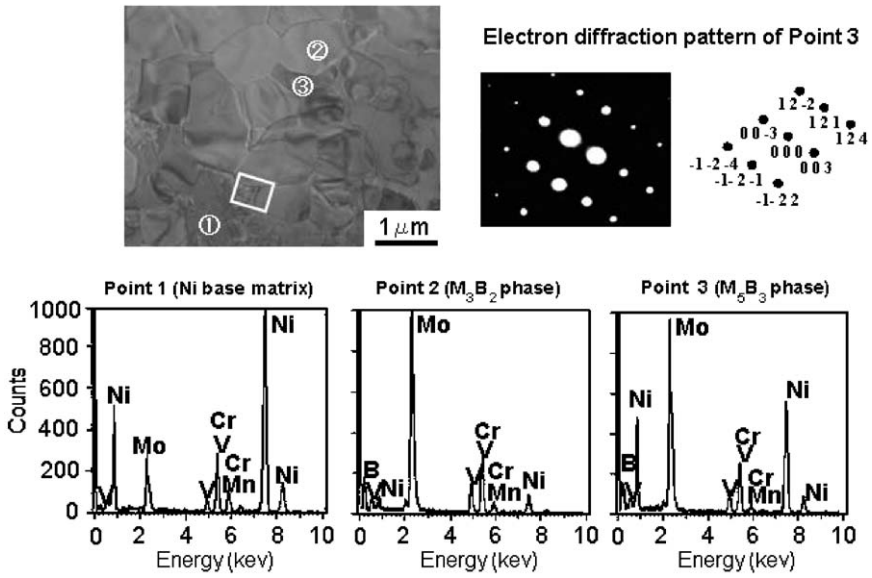


Fig. 20. Thin foil electron micrographs of Ni–5B–51Mo–12.5Cr–5V–3Mn mass% cermet and EDS analysis results at the marked points.

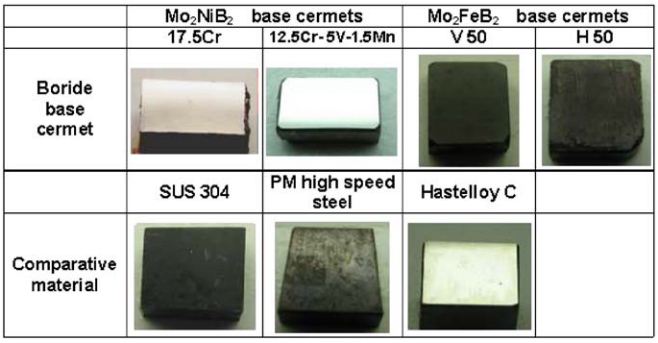


Fig. 21. Corrosion test result of $Mo_2NiB_2$ complex boride base cermets and comparative materials after dipped in molten fluorocarbon resin at 673 K for 259.2 ks (72 h).

thermoelectricity, etc. A unique sintering method of reaction boronizing sintering has successfully developed ternary boride-based cermets such as $Mo_2FeB_2$ and $Mo_2NiB_2$-based cermets. These cermets have excellent mechanical properties, corrosion and wear resistance and have been widely applied to practical uses such as injection molding machine parts, etc. It is to be expected that further applications of ternary boride-based cermets will be developed in the near future.

## References

[1] A. Leithe-Jasper, H. Klesner, P. Rogl, M. Komai, K. Takagi, J. Jpn. Inst. Met. 64 (2000) 154–162.
[2] K. Takagi, M. Komai, S. Matsuo, Proceedings of 1994 Powder Metallurgy World Congress (PM'94), SF2M and EPMA, Les Editions de Physique Les Ulis, France, vol. 1, 1994, p. 227–234.
[3] K. Takagi, Mater. Chem. Phys. 67 (2001) 214–219.
[4] K. Takagi, S. Ohira, T. Ide, T. Watanabe, Y. Kondo, Met. Powder Rep. 42 (1987) 483–490.
[5] M. Komai, Y. Yamasaki, K. Takagi, T. Watanabe, Properties of emerging P/M materials, advances in powder metallurgy & particulate materials, in: J.M. Capus, R.M. German (Eds.), Metal Powder Industries Federation, vol. 8, Princeton, New Jersey, USA, 1992, pp. 81–88.
[6] M. Komai, Y. Isobe, S. Ozaki, K. Takagi, in: Y. Bando, K. Kosuge, (Eds.), Proceedings of 1993 Powder Metallurgy World Congress, Japan Society of Powder and Powder Metallurgy, Kyoto, Japan, Part 2, 1993, pp. 1267–1270.
[7] Yu.B. Kuz'ma, M.V. Chepiga, Sov. Powder Met. 10 (82) (1969) 832–835.
[8] W. Reiger, H. Nowotny, F. Benesovsky, Monatsh. Chem. 97 (1966) 378–382.
[9] W. Reiger, H. Nowotny, F. Benesovsky, Monatsh. Chem. 95 (1964) 1502–1503.
[10] R. Warren, J. Mater. Sci. 3 (1968) 471–485.
[11] W.D. Klopp, J. Less Common Met. 42 (1975) 261–278.